

Rapid, Universal Surface Engineering of Carbon Materials via Microwave-Induced Carbothermal Shock

Geng Zhong, Shaomao Xu, Qi Dong, Xizheng Wang, and Liangbing Hu*

Carbon materials have been ubiquitously applied in energy conversion and storage devices owing to their high conductivity, excellent stability, and flexible structure. Conventional functionalization of carbon materials typically involves complex chemical treatment or long-term thermal and hydrothermal modifications. Here, **a one-step universal strategy for the rapid surface engineering of carbon materials by microwave-induced carbothermal shock is reported.** The temperature of carbon-fiber clothes (CC) quickly ramps to 1500 K within 5 s and maintains it for 2 s to complete the surface engineering process. At elevated temperatures, salt precursors decompose rapidly to form the catalytic nanoparticles, which simultaneously facilitate the oxidation of neighboring carbon sites, resulting in an activated CC with multiscale defects, oxygen-containing functional groups, and nanoparticles based on metal/metal oxide. In this process, both **high temperatures from carbothermal shock** and metal salt precursors are indispensable, as the former ensures effective carbon oxidation reaction while the latter provides the catalytic substance. The authors' method can be extended to many carbon materials, thereby offering a facile, efficient, and universal strategy for surface engineering toward a range of applications.

pristine carbon materials are typically inert with little functionalities on the surface, which necessitates further surface modification for practical applications.

For decades, tremendous efforts have been dedicated to developing surface modification strategies of carbon materials, among which the most widely adopted ones are chemical oxidation (e.g., oxidant oxidation and electrochemical oxidation) and thermal gasification (e.g., activation and heteroatomic doping). Chemical oxidation features superior universality to carbon materials, but usually involves strong oxidant as well as tedious post-treatments that lowers efficiency and raise safety and environmental concerns.^[16–18] On the other hand, thermal gasification treatment only require gaseous activating agent and programmed thermal treatment, which is facile, safe, and environment-friendly. Nevertheless, this method relies on the energy-inefficient and time-consuming thermal radiation process


1. Introduction

Carbon materials play an important role in energy conversion and storage owing to their superior advantages such as high conductivity, excellent stability, abundant sources, and flexible structure.^[1–5] The versatile carbon materials can not only serve as functional supports but also work individually as active substance in these systems.^[6–8] In most cases, the electrochemical performance depends largely on the surface physiochemical properties of carbon, as they can significantly affect the activities of carbon itself as well as the supported active materials. For example, heteroatom-doped carbon can display remarkably improved charge-storage capability^[9,10] and electrocatalytic performance.^[11,12] Meanwhile, carbon substrate with more defects and functional groups promotes smaller particle size and uniform distribution when used as conductive support for catalysis and electrochemical applications.^[13–15] However,

which results in a slow heating rate ($<1\text{ K s}^{-1}$).^[15,19] As a consequence, to achieve a high temperature (e.g., 1000 K), thermal gasification treatment typically requires tens of minutes or several hours, causing the limitation of its practical application. Lately, some new techniques emerge for the surface engineering of carbon materials such as laser etching^[20,21] and plasma spraying.^[22] While these techniques show improvement in terms of accuracy and efficiency, they are heavily dependent on the costly equipment and demanding operating conditions. Therefore, it is highly desirable to develop a facile, efficient, and universal strategy for surface engineering of carbon materials for practical applications.

It has been reported that carbon materials (e.g., graphene and graphite) can be catalytically etched under elevated temperatures by metal or metal oxide particles.^[23,24] Meanwhile, carbon materials are good microwave susceptors that can couple with microwave radiations and achieve ultrafast temperature ramping, namely microwave-induced carbothermal shock.^[25–27] By taking advantage of these two features, herein we report a rapid, universal surface engineering technique to functionalize carbon materials, which is enabled by microwave-induced carbonthermal shock with the in situ formed catalytic particles. During this process, the conductive carbon materials absorb electromagnetic energy to induce carbothermal shock, which ensures rapid decomposition of preloaded metal salt precursors and in situ catalytic etching of carbon. As a result,

Dr. G. Zhong, Dr. S. Xu, Dr. Q. Dong, Dr. X. Wang, Prof. L. Hu
Department of Materials Science and Engineering
University of Maryland
College Park, MD 20742, USA
E-mail: binghu@umd.edu

 The ORCID identification number(s) for the author(s) of this article can be found under <https://doi.org/10.1002/adfm.202010968>.

DOI: 10.1002/adfm.202010968

the intact and inert carbon surface can be rapidly functionalized with nanoparticles, defects, and active oxygen-containing functional groups. The whole processing only lasts for less than 10 s and is free of strong oxidant or hazardous chemicals, therefore is of high efficiency, good safety, and is environmentally benign. Furthermore, the reaction setup is simple and inexpensive (i.e., domestic microwave oven as reactor), making it easily accessible and scalable for mass production. By simply varying carbon substrates and metal salt precursors, our method enables rapid surface modification of a range of carbon materials with various surface structures. The microwave-induced carbothermal shock represents a facile, efficient, and universal strategy for surface engineering of carbon materials for a range of applications.

2. Results and Discussion

We use commercial carbon-fiber clothes (CC) and $\text{Cu}(\text{NO}_3)_2$ as starting materials to demonstrate the feasibility and utility of our rapid surface engineering approach. **Figure 1** shows the schematic of our strategy where the intact and inert surface of CC is rapidly functionalized with defects, nanoparticles, and active oxygen-containing functional groups. In a typical experiment, pristine CC were dipped into $\text{Cu}(\text{NO}_3)_2$ aqueous solution and dried at 80 °C to fabricate the CC/ $\text{Cu}(\text{NO}_3)_2$ precursor, which was then placed in an air-filled domestic microwave oven for carbothermal shock. During microwaving, the CC coupled with electromagnetic energy and triggered a rapid carbothermal shock, making the temperature rapidly ramp to ≈ 1500 K within 5 s (300 K s^{-1}) while emitting a dazzling light (Figure 1). The temperature

was maintained for ≈ 2 s, which was enough to achieve the functionalization of CC. As the temperature increased, the $\text{Cu}(\text{NO}_3)_2$ precursor first decomposed into CuO_x at ≈ 473 – 523 K, which further transferred to the mixture of Cu and Cu_2O catalytic nanoparticles at higher temperatures (>623 K).^[28] Under the peak temperature, the oxygen atoms around the catalytic nanoparticles participated in the in situ oxidation of the neighboring carbon species. Meanwhile, sufficient oxygen was supplied from air to afford a continuous and controlled carbon oxidation reaction, resulting in an activated CC with multiscale defects, oxygen-containing functional groups as well as the nanoparticles made of metal/metal oxide (Figure 1). Since both the microwave-induced carbothermal shock and catalytic oxidation are general behaviors for carbon, this rapid surface engineering approach can be readily extended to a variety of carbon substrates.

During the microwave-induced surface engineering, the conductive CC coupled with electromagnetic energy to trigger carbothermal shock, which instantly created tremendous heat and light emission. To study the temperature during carbothermal shock, the intensity of light emission was recorded by a high-speed camera, which was fitted to report the temperature map according to the black-body theory. To eliminate potential complications of microwave-induced non-black-body radiation (e.g., corona), we measured the temperature evolution of the initial ≈ 130 ms right after powering off the microwave, albeit the measured temperature could be slightly lower than the peak temperature during carbothermal shock. As shown in **Figure 2a**, the light intensity gradually decrease as a result of cessation of the input microwave energy, which demonstrates a fast cooling process as depicted by a series of real-time digital images (Figure 2a, inset). Based on the light intensity, the temperature

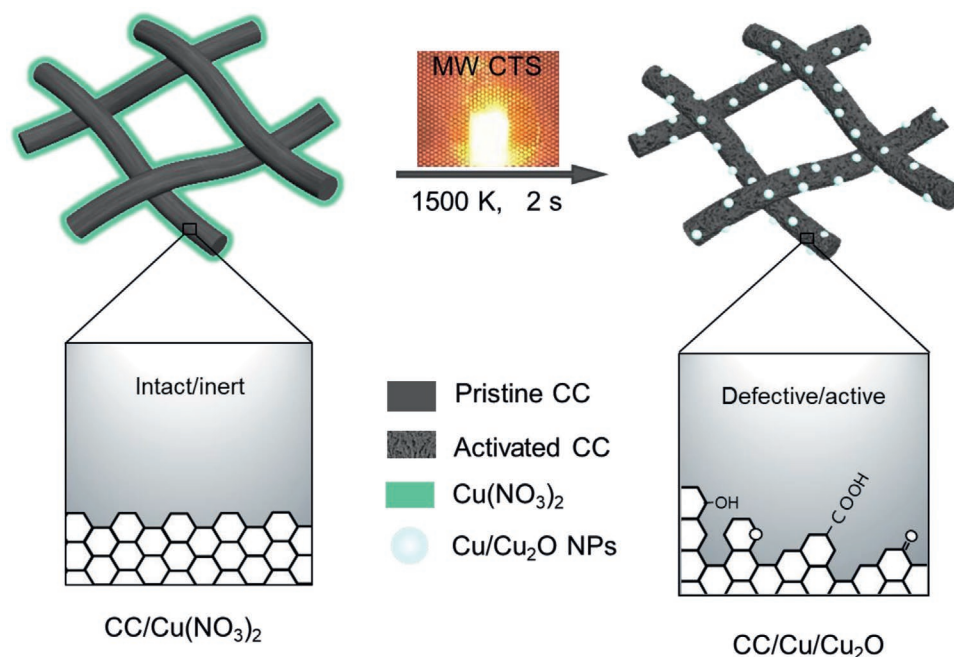


Figure 1. Schematic illustration of the rapid surface engineering of carbon materials. The pristine CC were dipped with $\text{Cu}(\text{NO}_3)_2$ precursor solution and then placed in an air-filled domestic microwave oven for **carbothermal shock**, which results in the activated CC with multiscale defects, oxygen-containing functional groups as well as the nanoparticles based on metal/metal oxide.

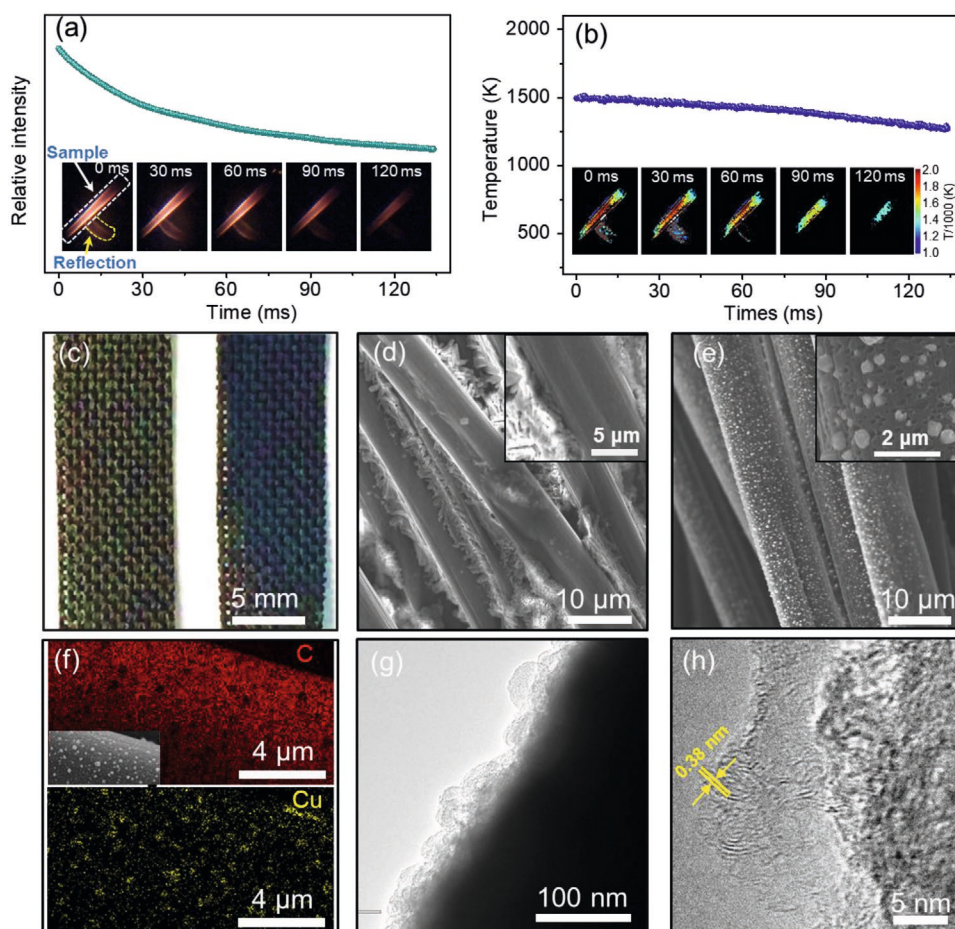


Figure 2. Characterization of the rapid surface engineering process. a) The emitted light intensity of CC as a function of time during microwave-induced carbothermal shock (Inset: the corresponding real-time digital images of the lighting CC in vial container with an optimized exposure. The light inside the white dashed line is the lighting sample while that inside the yellow dashed line is the reflection of the sample light in the vial wall. The photograph under natural light in Figure S5, Supporting Information, shows a more intuitive illustration). b) The temperature evolution of CC, calculated from light intensity according to the black-body theory (Inset: temperature profiles of the lighting CC in vial container fitted from high-speed pyrometry frames). c) Photo images of the CC/Cu(NO₃)₂ (left, before carbothermal shock) and CC/Cu/Cu₂O (right, after carbothermal shock). d) SEM image of CC/Cu(NO₃)₂ (Inset: magnified SEM). e) SEM image of CC/Cu/Cu₂O (Inset: magnified SEM). f) Elemental mapping of CC/Cu/Cu₂O. g) TEM images of CC/Cu/Cu₂O. h) The carbon bulges consisted of few-layer carbon nanosheets with an interplanar distance of 0.38 nm.

was fitted to be ≈ 1500 K when the microwave was stopped, suggesting a slightly higher temperature (>1500 K) during microwave carbothermal shock (Figure 2b). The calculated temperature profile displays a uniform temperature distribution of the sample, except for the two edge areas that were in contact with the reaction container (Figure 2b, inset). The high temperature and uniform temperature distribution achieved by the microwave-induced carbothermal shock ensures good homogeneity and high quality of surface engineering.

After modification, the original glossy CC turned matt (Figure 2c), which can be attributed to the higher roughness and surface modification. We performed the scanning electron microscopy (SEM) to investigate the morphology change of the sample. Prior to carbothermal shock, the Cu(NO₃)₂ precursors were mainly aggregated at the gaps between carbon fibers (Figure 2d), while the carbon fiber surface were mostly exposed (Figure 2d, inset). Owing to the short time of carbothermal shock (i.e., 2 s), the fabric structure (Figure 2c) and the integrity

of individual fibers were well preserved (Figure 2e). Meanwhile, the rapid thermal shock led to the fast decomposition and redispersion of Cu(NO₃)₂ precursors, resulting in uniform Cu-containing nanoparticles decorated on the carbon fibers (Figure 2e) as confirmed by energy dispersive X-ray spectroscopy mapping (Figure 2f). The particle size distribution of CC/Cu/Cu₂O was statistically analyzed. The average size of Cu/Cu₂O particles was 268.6 nm (Figure S1, Supporting Information), while the elemental Cu content was measured to be $\approx 4.87\%$ using thermogravimetric analysis (TGA) (Figure S2, Supporting Information). X-ray diffraction (XRD) patterns show that these nanoparticles consisted of Cu (PDF # 04-0836) and Cu₂O (PDF # 05-0067) (Figure S3, Supporting Information). Furthermore, compared with the original CC, the surface of carbon fiber is rough with numerous defective holes (Figure 2e, inset), indicating a uniform surface modification of CC. Transmission electron microscopy (TEM) images show that the surface of carbon fiber is coated with a layer of carbon bulges with a

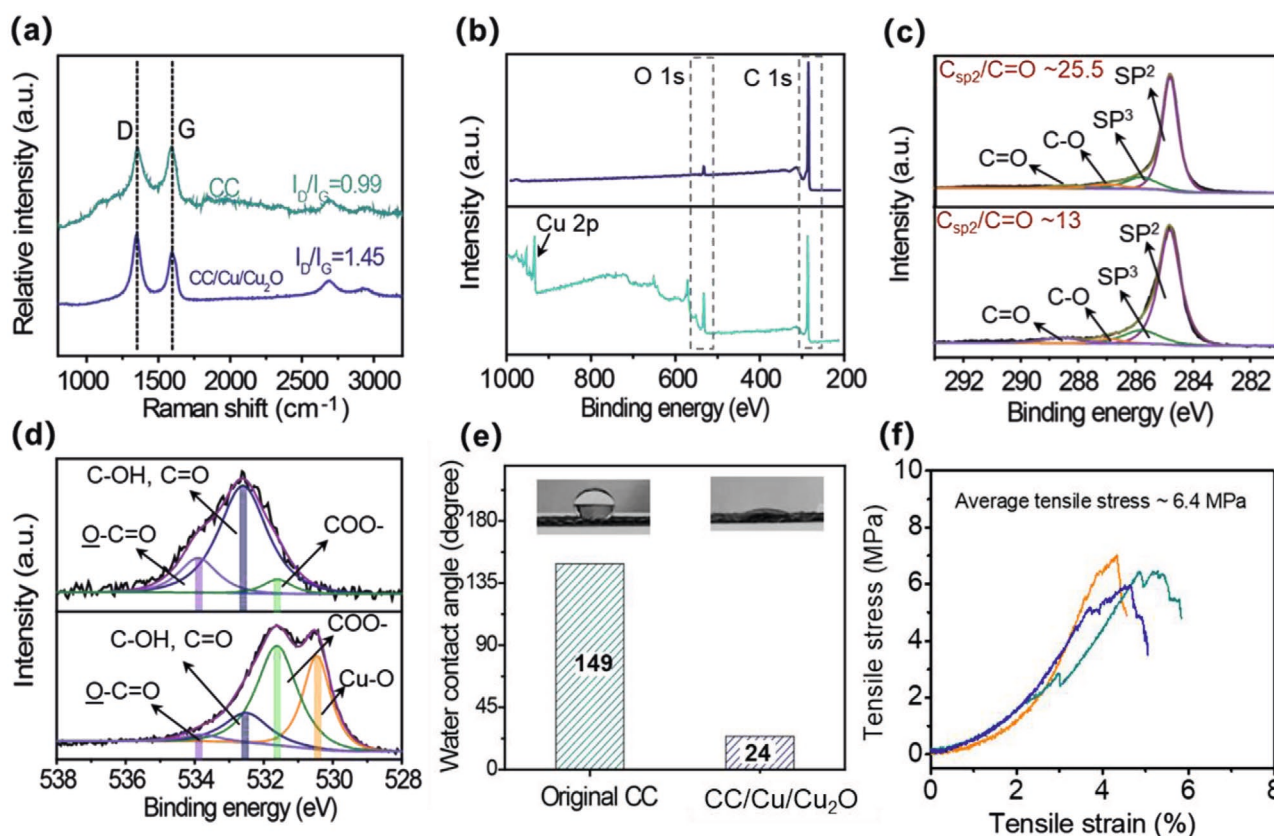


Figure 3. Characterization of the CC before and after surface engineering. a) Raman spectra, b) XPS survey spectra, c) C 1s, d) O 1s, and e) water contact angles of the CC before (top) and after (bottom) surface engineering. f) Tensile stress–strain curves of a set of three parallel CC samples after surface engineering.

diameter of $\sim 30\text{--}60$ nm. These carbon bulges consisted of few-layer carbon nanosheets with interplanar distance of 0.38 nm, a value larger than that of graphitic carbon in the original carbon fiber (i.e., $d_{002} = 0.34$ nm, Figure S4, Supporting Information). The fact that microwave-induced carbothermal shock leads to a significant change in the microstructure of CC with multiscale defects and nanoparticles decoration is confirmed.

We hypothesize that the rapid surface engineering is realized following the aforementioned catalytic oxidation mechanism of carbon at high temperature, where fast heating rate, short carbothermal shock duration, as well as catalytic nanoparticles play indispensable roles. To verify this hypothesis, we treated the CC/Cu(NO₃)₂ composite based on thermal radiation under 1500 K in an air-filled tube furnace, which has a much lower heating rate (typically <20 K s^{−1}) than that of the microwave-induced carbothermal shock.^[14] After 5 s of thermal radiation, the decomposition products were still unevenly aggregated in the gaps between carbon fibers (Figure S6, Supporting Information), suggesting a non-uniform surface engineering. This phenomenon is likely due to the low heating rate as well as the slow heat transfer which result in the lower temperature. The effect of carbothermal shock duration was studied by performing control experiments using heating times of 1 and 6 s. As shown in Figure S7, Supporting Information, the shorter heating duration (1 s) can lead to the decomposition of precursor and the generation of catalytic nanoparticles. However,

it is not enough to achieve the desirable surface modification of CC as can be evidenced by the intact surface of CC. In contrast, a longer shock duration leads to excessive oxidation of the carbon fiber, with the diameter of carbon fiber decreasing from ~ 9 to ~ 3 μm , which means a severe damage to its structure and integrity (Figure S8, Supporting Information). We also conducted a control experiment in which the bare CC with no salt precursor was treated in the same manner (i.e., with 2 s microwave carbothermal shock). The obtained CC showed negligible surface morphology change compared with the original CC, demonstrating the crucial role of in situ generated catalytic nanoparticles (Figure S9, Supporting Information). Taken together, these results indicate that high heating rate, short heating duration, as well as the catalytic nanoparticles are all indispensable for the surface engineering of carbon, which strongly agrees with our hypothesis.

Raman spectroscopy was used to investigate the defect level of CC before and after microwave-induced carbothermal shock. As shown in Figure 3a, two bands at 1350 and 1590 cm^{−1} are clearly identified in both samples, which correspond to the D band (defective carbon) and G band (sp² hybridized carbon) of carbon materials, respectively.^[29,30] Based on the Raman spectrum, the ratio of D band to G band (i.e., I_D/I_G) in the modified CC is calculated to be 1.45, which is much higher than that of the original CC (0.99), indicating a significantly increased content of defects. Figure 3b–d depicts the X-ray photoelectron

spectroscopy (XPS) spectra of the CC which reveal the changes of surface chemical compositions after the surface engineering. Both profiles show C 1s and O 1s peaks at 284.8 and 532.6 eV, respectively, while the Cu 2p peak (932.5 eV) is observed only in the modified samples which correspond to the newly generated nanoparticles. After modification, the intensity ratio of C/O (6.0, after eliminating the potential oxygen in Cu₂O) in CC is much lower than that in the original CC (23.3, Figure 3b), suggesting the formation of oxygen-containing functional groups on the surface. High-resolution XPS spectra were applied to further investigate the bonding states of C and O elements. As shown in Figure 3c, the C 1s peaks of both samples can be split into four peaks corresponding to graphitic C sp² (284.8 eV), aliphatic C sp³ (285.7 eV), C–O (286.9 eV), and O–C=O (288.6 eV) groups, respectively.^[20] After surface engineering, the ratio of C sp²/O–C=O of CC decreases from ≈25.5 to 13.0, indicating more oxidation of carbon. The O 1s spectrum of the original CC can be deconvoluted into three peaks corresponding to oxygen in carboxyl group (COO–, 531.6 eV), hydroxyl and carbonyl groups (C–OH and C=O, 532.5), and oxygen single bond in esters and carboxylic groups (O=C–O, 533.9 eV), respectively.^[20] Besides these peaks, a newly introduced metal–oxygen bond (Cu–O, 530.5 eV) can be observed for the modified CC, revealing the presence of Cu₂O. Moreover, the relatively increased COO– content can be clearly identified in the spectrum of the modified CC, which further demonstrates the enriched oxygen-containing functional groups.

Due to the improved content of defects and oxygen-containing functional groups, the wettability of CC was dramatically enhanced, as evidenced by the dramatic decrease of water contact angle from 149° to 24° after modification (Figure 3e). The recorded dynamic wetting process shows that water droplet can rapidly infiltrate into the modified CC within 0.8 s (Figure S10a). In comparison, the droplet remained unchanged on the surface of the original CC without obvious wetting even after 20 s (Figure S10b, Supporting Information). Despite the generated defects, the modified CC still exhibits a tensile stress of 6.4 MPa, a value that can afford good structural stability.

It has been reported that the Cu₂O and O heteroatom on the surface of carbon substrate can effectively guide the Li nucleation.^[31–33] In this work, we demonstrate the surface-engineered CC as a 3D lithiophilic current collector that spatially guide uniform Li deposition toward a stable dendrite-free Li metal anode. The voltage profiles (Figure S11, Supporting Information) show that the Li nucleation on CC/Cu/Cu₂O requires a much lower overpotential compared with original CC (16.5 vs 37.2 mV). As schematically depicted, Li metal uniformly nucleates onto the carbon fibers as guided by the lithiophilic surface, which further developed into a “self-smoothing” Li deposition process (Figure 4a). Initially, the surface of CC/Cu/Cu₂O is rough with nanoparticles and oxygen-containing functional groups (Figure 4b). These lithiophilic species can act as Li nucleation sites which lead to a uniform Li layer on the surface of CC/Cu/Cu₂O during the initial Li plating for 0.2 mAh cm^{–2} (Figure 4c). The cross-sectional SEM image shows more obvious coating layer onto the entire surface of fibers (Figure 4c inset), which further confirms the good uniformity of Li nucleation. During further plating, the growth of Li from the nucleation gradually filled the holes, forming a smooth dendrite-free Li metal anode

after Li deposition for 2 mAh cm^{–2} (Figure 4d and inset). In contrast, the surface of original CC is smooth without lithiophilic nanoparticles (Figure 4e). Consequently, instead of nucleating on CC, the Li inclined to grow at the open space between fibers thus forming unevenly distributed agglomerates (Figure 4f). As the plating proceeds, Li ions tend to deposit on the existed Li nuclei, which result in the pillar-like Li grown outside the carbon fiber (Figure 4g and inset). XRD analysis was conducted to investigate the changes of material during the lithiation process (Figure S12, Supporting Information). The XRD pattern of CC/Cu/Cu₂O reveals three phases in CC/Cu/Cu₂O, which were graphitic C, Cu, and Cu₂O. When the discharge capacity reached to 2 mAh cm^{–2}, the peak of Li (2θ = 36.1°) (PDF#15-0401) was detected, indicating the plating of Li metal. Meanwhile, the peak of Cu₂O disappeared after lithiation, while the peak of Li₂O (2θ = 33.4°) (PDF#12-0254) was detected. We infer that during Li deposition, the lithiophilic Cu₂O reacted with the plated Li and generate Cu and Li₂O, which facilitated the Li nucleation and the following uniform Li deposition processes. Besides, the peak of Li_xC_y (2θ at 22°–24.5°) was also identified, suggesting the lithiation of carbon during the discharge process. The lithiation of carbon also account for the relatively large capacity when discharge voltage was above 0 V versus Li⁺/Li.

The Li stripping/plating behavior has a profound impact on the electrochemical performance of the Li metal battery. The composite electrodes, CC@Li and CC/Cu/Cu₂O@Li, were constructed by depositing 3 mAh cm^{–2} of Li, which were then assembled into symmetric testing cells for electrochemical characterization. As shown in Figure 5a, the cell based on CC/Cu/Cu₂O@Li displayed stable and low overpotential of ≈34 mV at 0.5 mA cm^{–2} for 380 cycles with good stability (Figure 5a). Although the overpotential of CC@Li symmetric cell was also stable in the initial 200 cycles, it increased dramatically since then, and short circuited after 330 cycles. The increase of overpotential was likely due to the large nucleation barrier of Li as a result of the poor lithiophilicity.^[34,35] Figure 5b shows the voltage profiles of both symmetric cells tested at various current densities (0.5, 1.0, 2.0, and 5.0 mA cm^{–2}) to reach the same capacity of 1 mAh cm^{–2}. Compared with the CC@Li cell, the CC/Cu/Cu₂O@Li cell exhibited lower overpotentials at all the testing current densities, further confirming the superior stability and rate performance. The Li plating on CC/Cu/Cu₂O shows a significantly decreased overpotential, indicating the guiding effect by Cu₂O nanoparticles and oxygen-containing functional groups for Li nucleation and deposition.

To further demonstrate the potential of the modified CC as Li host in practical Li batteries, we tested full cells by using the as-prepared composite anode, LiNi_{0.5}Mn_{0.3}Co_{0.2}O₂ (NMC) cathode, and carbonate-based electrolyte. Cyclic voltammetry was tested at 0.1 mV s^{–1} scanning from 3.0 to 4.3 V to study the Li-ion diffusion kinetics of the test cells. As shown in Figure 5c, the characteristic peaks of NMC can be observed in both cells, while the overpotential (voltage difference between anodic and cathodic peak) of the CC/Cu/Cu₂O@Li|NMC cell is smaller than that of the CC@Li|NMC cell, indicating its lower polarization and better reaction kinetics.^[36] The smaller overpotential of the CC/Cu/Cu₂O@Li|NMC cell is consistent with its smaller voltage gap between charge and discharge plateau (Figure 5d). As the cathode and electrolyte are identical in both cells, the

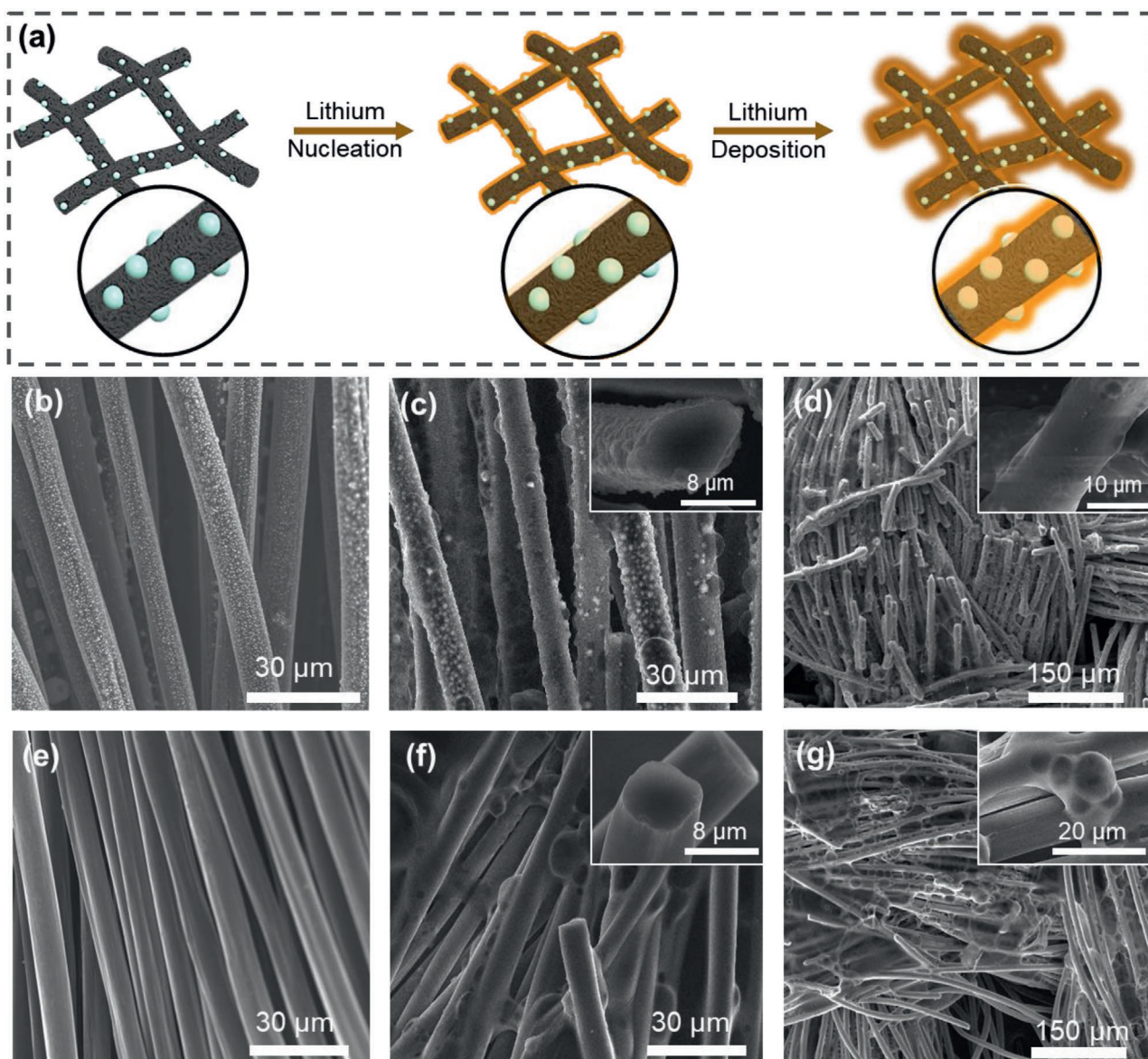


Figure 4. a) Schematics of guided Li nucleation and deposition on surface of engineered CC. SEM images of pristine CC/Cu/Cu₂O with b) no Li deposition, c) 0.2 mAh cm⁻² of Li uniformly nucleated on surface CC/Cu/Cu₂O, and d) 2 mAh cm⁻² of Li plated on CC/Cu/Cu₂O (insets are corresponding cross-sectional SEM images showing the uniform Li nucleation and plating). e) SEM images of control samples of original CC with no surface engineering, f) 0.2 mAh cm⁻² of Li unevenly nucleated on original CC, and g) 2 mAh cm⁻² of Li unevenly plated on original CC.

improved electrochemical performance of the CC/Cu/Cu₂O@Li|NMC cell is likely attributed to the lithiophilic surface of CC/Cu/Cu₂O substrate that favors uniform Li deposition.

Benefited from the superior electrochemical stability of the CC/Cu/Cu₂O@Li anode, its full cell displayed a high capacity of 151 mAh g⁻¹ when cycled at 0.5 C (80 mA g⁻¹) for 200 cycles, with a capacity retention of 94.1%, which is much better than the cell based on CC@Li anode (69 mAh g⁻¹ for 100 cycles, with capacity retention of 41.8%, Figure 5e). Furthermore, the average Coulombic efficiency of the CC/Cu/Cu₂O@Li|NMC cell from the second cycle reached as high as 99.06%, suggesting good reversibility. The rate performance of the two cells was investigated by cycling the test cells at rates of 0.2, 0.5, 1, and 2 C. The corresponding specific capacities of the CC/Cu/Cu₂O@Li|NMC cell

were 160.1, 154.2, 143.6, and 124.1 mAh g⁻¹, respectively, which were higher than those of the CC@Li|NMC cell (155.4, 140.2, 109.1, and 61.0, respectively, Figure 5f). After resetting the current density back to 0.2 C, the CC/Cu/Cu₂O@Li|NMC cell still maintained the original capacity of ≈160 mAh g⁻¹, while the CC@Li|NMC cell displayed a dramatically decreased capacity of ≈120 mAh g⁻¹ (Figure 5f). The improved battery performance using the CC/Cu/Cu₂O@Li anode further confirms the importance of surface engineering on carbon substrate by the microwave-induced carbothermal shock.

Note the application of surface-engineered carbon materials is not limited to Li metal batteries, but can be extended to water purification,^[37,38] composite reinforcement,^[39,40] gas separation (e.g., CO₂ capture)/storage,^[41,42] electrochemical catalysts,^[11,12]

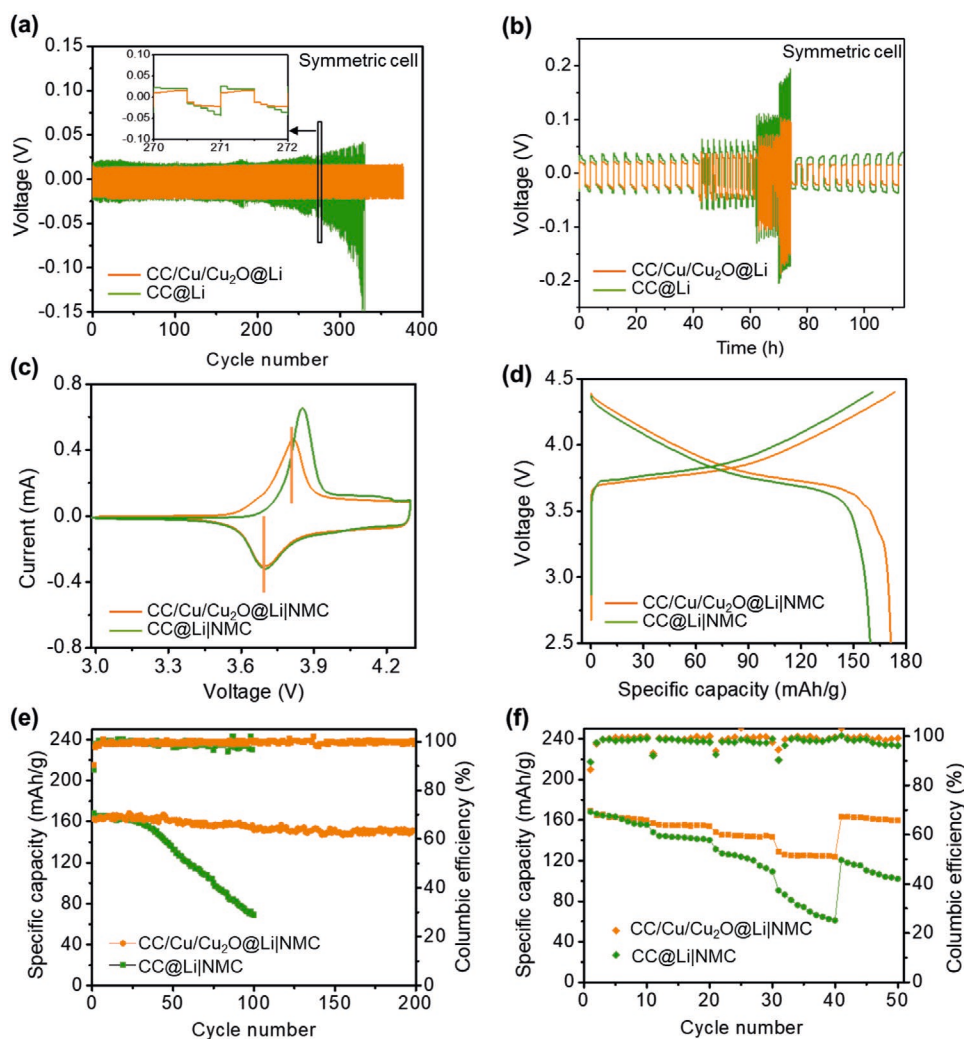


Figure 5. Electrochemical characterizations based on different composite anodes. Voltage profiles of the CC@Li|NMC and CC/Cu/Cu₂O@Li symmetric cells to show a) cycling stability at 0.5 mA cm⁻² and b) rate performance at various current densities of 0.5, 1, 2, and 5 mA cm⁻². Electrochemical performance of the CC@Li|NMC and CC/Cu/Cu₂O@Li|NMC full cells. c) CV curves at 0.1 mA g⁻¹, d) charge-discharge curves at 0.2 C, e) cycling performance at 0.2 C, and f) rate capacity recorded from 0.2 to 2 C.

and other energy conversion technologies.^[43,44] Here, we also demonstrate the potential applications of this strategy in the fields of supercapacitors and dye absorption. Figure S13, Supporting Information, shows that the symmetric supercapacitor with CC/Cu/Cu₂O as electrode showed remarkably improved capacity at various scan rates while Figure S14, Supporting Information, proves that the CC/Cu/Cu₂O material can purify contaminated water much more effectively.

As the catalytic etching under high temperatures is a general behavior for carbon, the rapid surface engineering therefore possesses great versatility when applying different catalysts or on various carbon substrates. Using Ni(NO₃)₂ as precursor of catalytic nanoparticles, the surface of carbon fiber can be decorated with a layer of fluffy carbon nanotubes (Figure 6a), which can be clearly observed in the magnified SEM image (Figure 6a, inset). In other examples, aligned channels were achieved when applying Co(NO₃)₂ precursor (Figure 6b), while broad and random etching trenches was obtained when using Zn(NO₃)₂

(Figure 6c). The formation of these versatile surface structures is likely due to the different catalytic properties of the catalytic nanoparticles. We also verified the universality of this surface engineering strategy through modifying carbon materials with various structures including 1D carbon fiber (Figure 6d), 2D graphite flakes (Figure 6e), and 3D carbonized wood (Figure 6f). After microwave-induced carbothermal shock with metal salt precursors, these materials are successfully engineered with defects (e.g., grooves, holes and pores) as well as active nanoparticles (Figure 6d–f). Compared with conventional surface modification techniques, the rapid microwave-induced carbothermal shock features superior operation simplicity and much shorter processing time, which can be readily integrated with the well-developed roll-to-roll processes for scalable production. As a proof-of-concept, we show in Figure 6g that the carbon material is first soaked in a precursor bath, and then passed through a microwave radiation cavity, where the carbothermal shock was rapidly triggered to achieve surface engineering.

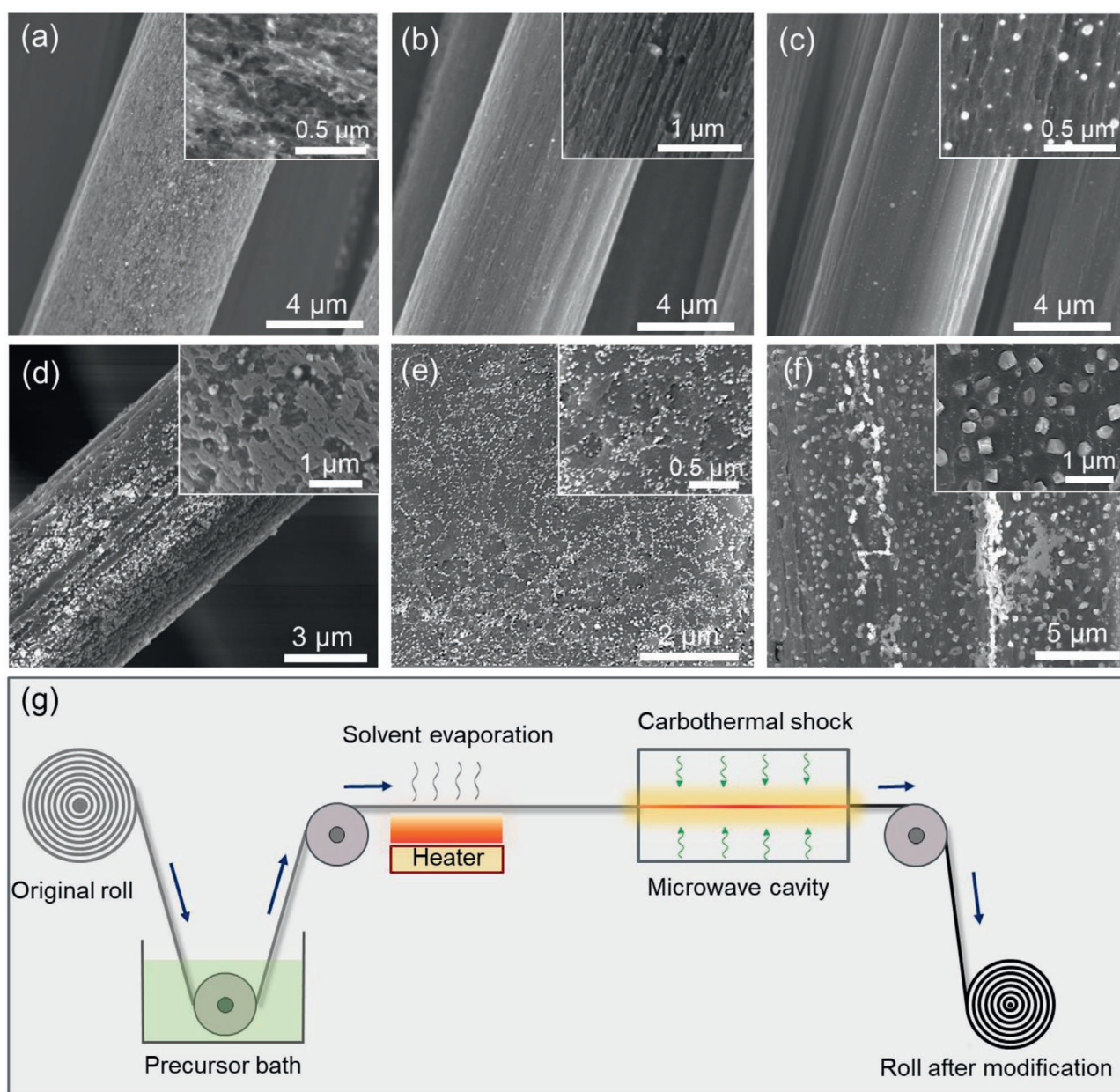


Figure 6. Versatility and universality of the microwave-induced carbothermal shock. Surface engineering of CC achieved by using different precursors, including: a) $\text{Ni}(\text{NO}_3)_2$, b) $\text{Co}(\text{NO}_3)_2$, and c) $\text{Zn}(\text{NO}_3)_2$. Surface engineering of carbon materials with various structures to show the universality of the microwave carbothermal shock, including: d) carbon fiber (with AgNO_3 precursor), e) graphite flake (with AgNO_3 precursor), and f) carbonized wood (with $\text{Cu}(\text{NO}_3)_2$ precursor). g) Schematic illustration of a roll-to-roll manufacturing process for the surface engineering of carbon materials.

3. Conclusion

In summary, we have for the first time demonstrated a microwave-induced carbothermal shock strategy for rapid surface engineering of carbon materials, which can quickly introduce defects, catalytic nanoparticles and oxygen-containing functional groups. Using $\text{CC}/\text{Cu}(\text{NO}_3)_2$ as a model system, we have proved that the rapid surface engineering is based on the catalytic oxidation mechanism of carbon at high temperatures, in which the fast heating rate, short shock duration, as well as catalytic

nanoparticles play indispensable roles. The CC exhibited significantly improved electrochemical performance after surface engineering when used as the substrate for Li metal anode. The microwave-induced carbothermal shock can be extended to construct a range of surface structures on carbon-based materials through rational selection of catalyst precursors. We have also demonstrated the excellent universality of this surface engineering strategy by varying carbon materials with different structures including 1D carbon fiber, 2D graphite flake, and 3D carbonized wood. The simple and efficient microwave-induced

carbothermal shock approach can potentially be integrated with the well-developed roll-to-roll process for continuous surface engineering of carbon materials in large scale.

4. Experimental Section

Materials: $\text{Cu}(\text{NO}_3)_2 \cdot 3\text{H}_2\text{O}$ (>98%), $\text{Ni}(\text{NO}_3)_2 \cdot 6\text{H}_2\text{O}$ (>97%), $\text{Co}(\text{NO}_3)_2 \cdot 6\text{H}_2\text{O}$ (>98%), $\text{Zn}(\text{NO}_3)_2 \cdot 6\text{H}_2\text{O}$ (>98%), and $\text{AgNO}_3 \cdot 6\text{H}_2\text{O}$ (>99%) salt precursors, polyvinylidene difluoride (PVDF), *N*-Methylpyrrolidone, lithium hexafluorophosphate solution (1.0 M LiPF_6 in EC [50%] and DEC [50%]), and Li foil were purchased from Sigma-Aldrich. Plain CC and carbon fiber were purchased from Fuel Cell Store. Graphite was purchased from Asbury Carbons. NMC cathode was provided by TODA America, USA. Carbon black (C45 CB) was purchased from Imerys Graphite & Carbon, Switzerland.

Surface Engineering of Carbon Materials: CC (8 mm \times 32 mm) were immersed into 0.5 M $\text{Cu}(\text{NO}_3)_2$ precursor solution, vacuum infiltrated, and dried at 60 °C to form CC/ $\text{Cu}(\text{NO}_3)_2$. Afterward, the CC/ $\text{Cu}(\text{NO}_3)_2$ was placed in a vial before being exposed to a 1000 W microwave radiation for 4 s in a domestic oven (Panasonic). The duration of surface engineering could be easily adjusted by changing the time of microwaving.

Materials Characterization: The morphologies were captured on a field-emission SEM (Hitachi SU-70) and a TEM (FEI Tecnai G2 F20 S-Twin). The size distribution of particle was analyzed with an ImageJ image processing program. XRD characterization was conducted using a D8 system with a Cu K α radiation ($\lambda = 1.5418$ Å, Bruker AXS). Raman analysis was performed using a 532-nm laser excitation, 4 s integration time, and 4 repeated tests (Horiba Jobin-Yvon). Surface chemical compositions were detected by XPS (ESCALab250). TGA analysis was performed with TA Instruments (Q500) from 30 to 800 °C in air with a heating rate of 5 °C min⁻¹. The dye adsorption performance of CC materials was investigated by the static adsorption of methylene blue. Typically, the CC materials with an area of 0.5 cm² were immersed in 6 mg L⁻¹ methylene blue solution to conduct the dye adsorption for 2 h. After that, the UV-vis spectrum of the resultant solutions was measured on a Specord 200 (Analytik Jena AG) with a wavelength from 400 to 800 nm. The temperature during microwaving was measured following the authors' previous work.^[26] The light emission of microwave-induced carbothermal shock was captured by a high-speed camera (Vision Research Phantom Miro M110) and calibrated with a Newport Oriel 67000 Series Blackbody Infrared Light Source.

Electrochemical Characterization: Standard CR2032 coin cells were employed to investigate the electrochemical performance. The Celgard membrane and 1.0 M LiPF_6 (in EC and DEC with volume ratio of 1:1) was used as separator and electrolyte, respectively. The Li metal composite anode was obtained by conducting 3 mAh cm⁻² of Li deposition in the CC or CC/ $\text{Cu}/\text{Cu}_2\text{O}$ electrode. The symmetric cells using Li metal composite as electrode was assembled and cycled with a capacity of 0.5 mAh cm⁻² and current density of 0.5 mA cm⁻² to study the Li plating/stripping behavior. The rate performance of the symmetric cell was tested at current densities of 0.5, 1, 2, and 5 mA cm⁻² with a capacity of 1 mAh cm⁻². In the practical batteries system, composite Li anode was coupled with NMC532 cathode. The cathode was fabricated following the classic blade coating method which contains NMC532, carbon black, and PVDF with a mass ratio of 8:1:1. The cathode composite was coated on Al foil with a mass loading of 5 mg cm⁻². The cyclic voltammetry curves were recorded via a CHI660E electrochemical workstation (CH Instruments), and the galvanostatic cycling were tested by a Land system. The supercapacitor performance of CC materials was investigated via a three-electrode system which consisted of CC materials as working electrode, Pt plate as counter electrode, Ag|AgCl as reference electrode and 3 M KOH solution as electrolyte.

Supporting Information

Supporting Information is available from the Wiley Online Library or from the author.

Acknowledgements

This work has no direct funding support. The authors acknowledge the use and support of the Maryland NanoCenter and its AIM Lab.

Conflict of Interest

The authors declare no conflict of interest.

Author Contributions

G.Z. conducted the material synthesis and characterizations with the help of S.X. X.W. contributed to the temperature measurement. G.Z. analyzed the data. G.Z., Q.D., and L.H. collectively wrote the paper with input from all authors.

Data Availability Statement

Research data are not shared.

Keywords

carbothermal shock, lithium metal batteries, microwaves, surface engineering, three-dimensional lithium hosts

Received: December 21, 2020
Published online: February 24, 2021

- [1] M.-M. Titirici, R. J. White, N. Brun, V. L. Budarin, D. S. Su, F. D. Monte, J. H. Clark, M. J. MacLachlan, *Chem. Soc. Rev.* **2015**, *44*, 250.
- [2] X. Wang, A. Vasileff, Y. Jiao, Y. Zheng, S.-Z. Qiao, *Adv. Mater.* **2019**, *31*, 1803625.
- [3] M. R. Benziger, S. N. Talapaneni, S. Joseph, K. Ramadass, G. Singh, J. Scaranto, U. Ravon, K. Al-Bahily, A. Vinu, *Chem. Soc. Rev.* **2018**, *47*, 2680.
- [4] C. Hu, L. Dai, *Adv. Mater.* **2019**, *31*, 1804672.
- [5] Y. G. Lee, S. Fujiki, C. Jung, N. Suzuki, N. Yashiro, R. Omoda, D. S. Ko, T. Shiratsuchi, T. Sugimoto, S. Ryu, J. H. Ku, T. Watanabe, Y. Park, Y. Aihara, D. Im, I. T. Han, *Nat. Energy* **2020**, *5*, 299.
- [6] G. Zhong, S. Xu, M. Cui, Q. Dong, X. Wang, Q. Xia, J. Gao, Y. Pei, Y. Qiao, G. Pastel, *Small* **2019**, *15*, 1904881.
- [7] J. Yu, W. Lu, J. P. Smith, K. S. Booksh, L. Meng, Y. Huang, Q. Li, J.-H. Byun, Y. Oh, Y. Yan, T.-W. Chou, *Adv. Energy Mater.* **2017**, *7*, 1600976.
- [8] Y. Zhang, Y. Shi, X. C. Hu, W. P. Wang, R. Wen, S. Xin, Y. G. Guo, *Adv. Energy Mater.* **2020**, *10*, 1903325.
- [9] W. Wang, W. Liu, Y. Zeng, Y. Han, M. Yu, X. Lu, Y. Tong, *Adv. Mater.* **2015**, *27*, 3572.
- [10] Z. Li, Z. Xu, H. Wang, J. Ding, B. Zahiri, C. M. B. Holt, X. Tan, D. Mitlin, *Energy Environ. Sci.* **2014**, *7*, 1708.
- [11] Z. Lu, G. Chen, S. Siahrostami, Z. Chen, K. Liu, J. Xie, L. Liao, T. Wu, D. Lin, Y. Liu, T. F. Jaramillo, J. K. Nørskov, Y. Cui, *Nat. Catal.* **2018**, *1*, 156.
- [12] D. Guo, R. Shibuya, C. Akiba, S. Saji, T. Kondo, J. Nakamura, *Science* **2016**, *351*, 361.
- [13] Y. Yao, Z. Huang, P. Xie, T. Li, S. D. Lacey, M. Jiao, H. Xie, K. K. Fu, R. J. Jacob, D. J. Kline, Y. Yang, M. R. Zachariah, C. Wang,

- R. Shahbazian-Yassar, L. Hu, *ACS Appl. Mater. Interfaces* **2019**, *11*, 29773.
- [14] Y. Yao, Z. Huang, P. Xie, S. D. Lacey, R. Jacob, H. Xie, F. Chen, A. Nie, T. Pu, M. Rehwoldt, D. Yu, M. R. Zachariah, C. Wang, R. Shahbazian-Yassar, J. Li, L. Hu, *Science* **2018**, *359*, 1489.
- [15] Y. Qiao, S. Xu, Y. Liu, J. Dai, H. Xie, Y. Yao, X. Mu, C. Chen, D. J. Kline, E. M. Hitz, B. Liu, J. Song, P. He, M. R. Zachariah, L. Hu, *Energy Environ. Sci.* **2019**, *12*, 1100.
- [16] K. A. Wepasnick, B. A. Smith, K. E. Schrote, H. K. Wilson, S. R. Diegelmann, D. H. Fairbrother, *Carbon* **2011**, *49*, 24.
- [17] N. Karousis, N. Tagmatarchis, D. Tasis, *Chem. Rev.* **2010**, *110*, 5366.
- [18] J. Chen, B. Yao, C. Li, G. Shi, *Carbon* **2013**, *64*, 225.
- [19] W. Y. Ao, J. Fu, X. Mao, Q. H. Kang, C. M. Ran, Y. Liu, H. D. Zhang, Z. P. Gao, J. Li, G. Q. Liu, J. J. Dai, *Renewable Sustainable Energy Rev.* **2018**, *92*, 958.
- [20] Z. Liu, Z. Zhao, Y. Wang, S. Dou, D. Yan, D. Liu, Z. Xia, S. Wang, *Adv. Mater.* **2017**, *29*, 1606207.
- [21] W. Zhang, Y. Lei, Q. Jiang, F. Ming, P. M. F. J. Costa, H. N. Alshareef, *Small Methods* **2019**, *3*, 1900005.
- [22] F. Liu, H. Li, S. Gu, X. Yao, Q. Fu, *Surf. Coat. Technol.* **2019**, *374*, 966.
- [23] J. Wan, L. Huang, J. Wu, L. Xiong, Z. Hu, H. Yu, T. Li, J. Zhou, *Adv. Funct. Mater.* **2018**, *28*, 1800382.
- [24] N. Severin, S. Kirstein, I. M. Sokolov, J. P. Rabe, *Nano Lett.* **2009**, *9*, 457.
- [25] D. Voiry, J. Yang, J. Kupferberg, R. Fullon, C. Lee, H. Y. Jeong, H. S. Shin, M. Chhowalla, *Science* **2016**, *353*, 1413.
- [26] S. Xu, G. Zhong, C. Chen, M. Zhou, D. J. Kline, R. J. Jacob, H. Xie, S. He, Z. Huang, J. Dai, A. H. Brozena, R. Shahbazian-Yassar, M. R. Zachariah, S. M. Anlage, L. Hu, *Matter* **2019**, *1*, 759.
- [27] A. M. Schwenke, S. Hoepfner, U. S. Schubert, *Adv. Mater.* **2015**, *27*, 4113.
- [28] I. V. Morozov, K. O. Znamenkov, Y. M. Korenev, O. A. Shlyakhtin, *Thermochim. Acta* **2003**, *403*, 173.
- [29] D. Guo, J. Qin, Z. Yin, J. Bai, Y.-K. Sun, M. Cao, *Nano Energy* **2018**, *45*, 136.
- [30] M.-S. Balogun, W. Qiu, F. Lyu, Y. Luo, H. Meng, J. Li, W. Mai, L. Mai, Y. Tong, *Nano Energy* **2016**, *26*, 446.
- [31] Y. Ma, Y. Gu, Y. Yao, H. Jin, X. Zhao, X. Yuan, Y. Lian, P. Qi, R. Shah, Y. Peng, Z. Deng, *J. Mater. Chem. A* **2019**, *7*, 20926.
- [32] Y. Liu, X. Qin, S. Zhang, Y. Huang, F. Kang, G. Chen, B. Li, *Energy Storage Mater.* **2019**, *18*, 320.
- [33] X. Chen, X. R. Chen, T. Z. Hou, B. Q. Li, X. B. Cheng, R. Zhang, Q. Zhang, *Sci. Adv.* **2019**, *5*, eaau7728.
- [34] R. Zhang, X. Chen, X. Shen, X. Q. Zhang, X. R. Chen, X. B. Cheng, C. Yan, C. Z. Zhao, Q. Zhang, *Joule* **2018**, *2*, 764.
- [35] C. Niu, H. Pan, W. Xu, J. Xiao, J. G. Zhang, L. Luo, C. Wang, D. Mei, J. Meng, X. Wang, Z. Liu, L. Mai, J. Liu, *Nat. Nanotechnol.* **2019**, *594*, 594.
- [36] B. Liu, Y. Zhang, G. Pan, C. Ai, S. Deng, S. Liu, Q. Liu, X. Wang, X. Xia, J. Tu, *J. Mater. Chem. A* **2019**, *7*, 21794.
- [37] S. Bolisetty, R. Mezzenga, *Nat. Nanotechnol.* **2016**, *11*, 365.
- [38] Y. Yang, R. Zhao, T. Zhang, K. Zhao, P. Xiao, Y. Ma, P. M. Ajayan, G. Shi, Y. Chen, *ACS Nano* **2018**, *12*, 829.
- [39] J. Yu, L. Meng, D. Fan, C. Zhang, F. Yu, Y. Huang, *Composites, Part B* **2014**, *60*, 261.
- [40] M. Zhao, L. Meng, L. Ma, L. Ma, X. Yang, Y. Huang, J. E. Ryu, A. Shankar, T. Li, C. Yan, Z. Guo, *Compos. Sci. Technol.* **2018**, *154*, 28.
- [41] A. Alabadi, S. Razzaque, Y. Yang, S. Chen, B. Tan, *Chem. Eng. J.* **2015**, *281*, 606.
- [42] H. Richter, H. Voss, N. Kaltenborn, S. Kämnitz, A. Wollbrink, A. Feldhoff, J. Caro, S. Roitsch, I. Voigt, *Angew. Chem., Int. Ed.* **2017**, *56*, 7760.
- [43] H. Im, T. Kim, H. Song, J. Choi, J. S. Park, R. Ovalle-Robles, H. D. Yang, K. D. Kihm, R. H. Baughman, H. H. Lee, T. J. Kang, Y. H. Kim, *Nat. Commun.* **2016**, *7*, 10600.
- [44] M. Ye, Z. Zhang, Y. Zhao, L. Qu, *Joule* **2018**, *2*, 245.